Inorganic Chemistry
Article

*Inorg. Chem.* **2009**, *48*, 6501–6508 **6501**
DOI: 10.1021/ic9003164

# Photophysics of Heteroleptic Iridium(III) Complexes Of Current Interest; a Closer Look on Relaxation Dynamics

**Hsin-Sheng Duan,[†] Pi-Tai Chou,*[,†] Cheng-Chih Hsu,[†] Jui-Yi Hung,[‡] and Yun Chi*[,‡]**

[†]*Department of Chemistry, National Taiwan University, No. 1, Section 4, Roosevelt Road, Taipei 10617, Taiwan, R.O.C, and* [‡]*Department of Chemistry, National Tsing Hua University, 101, Section 2, Kuang Fu Road, Hsinchu 30013, Taiwan, R.O.C*

Received February 16, 2009

The excited-state dynamics of heteroleptic iridium(III) complexes have been investigated using femto-nanosecond time-resolved luminescence and transient absorption spectroscopy. Two prototypical examples illustrated here are iridium(III) bis[2-(2,4-difluorophenyl)pyridinato-N,$C^{2'}$] quinaldinate (**1**) and iridium(III) bis[2-(2,4-difluorophenyl)pyridinato-*N*,$C^{2'}$]-[2-(6-methylbenzoxazol-2-yl)phenolate] (**2**). Upon photoexcitation at, for example, 400 nm, the emission decay, monitored at the region of phosphorescence, for both **1** and **2** consists of a system response limited rise (<300 ps) and a single exponential decay. Further single wavelength as well as full spectrum of femto-picosecond transient absorption acquired in $CH_2Cl_2$ at room temperature reveals an ultrafast $S_1 \rightarrow T_n$ intersystem crossing (<1 ps) and a rapid $T_n \rightarrow T_1$ internal conversion/vibrational relaxation within a time period of <10 ps. The results lead us to conclude that following Franck−Condon excitation, the time scale required to populate the lowest triplet state should be <10 ps.

## Introduction

Because of their potential in improving device performances, organic light-emitting diodes (OLEDs) based on phosphorescence transition metal complexes have been receiving great attention.[1] In theory, the internal quantum efficiency of phosphorescent OLEDs can reach an upper limit of unity, rather than the maximum of 25% inherently imposed by the formation of singlet excitons for their fluorescent counterparts.[2] Accordingly, a large amount of effort has been made in investigating the second and third-row transition-metal complexes, aimed at development of highly efficient phosphors that can emit all three primary colors. The strong spin−orbit coupling expected for these heavy-metal ions would result in a fast intersystem crossing from the singlet excited state to the triplet manifold. Furthermore, mixing of singlet and triplet excited states through spin−orbit coupling, to a large extent, would also partially remove the spin-forbidden nature of the $T_1 \rightarrow S_0$ radiative relaxation, which leads to a fast radiative decay, so that quenching and/or annihilation processes can be comparably small, resulting in highly intense phosphorescent emission.[3]

As for the Ir(III) based complexes, tuning of emission colors over entire visible spectra has been achieved by modification of both heterocyclic cyclometalates and/or third chelating anions that are generally represented by C^N and L^X, respectively.[4] In one system, color tuning over a visible range from 440 to 596 nm was achieved by simple variation of L^X chromophores.[5] Furthermore, cationic Ir(III) complexes containing two phenylpyrazolic cyclometalates and a third diimine chelate were also synthesized and tested for light-emitting electrochemical cells.[6]

*To whom correspondence should be addressed. E-mail: chop@ntu.edu.tw (P.-T.C.), ychi@mx.nthu.edu.tw (Y.C.). Phone: +886-2-33663894 (P.-T.C.), +886-3-5712956 (Y.C.). Fax: +886-2-23695208 (P.-T.C.), +886-3-5720864 (Y.C.).

(1) (a) Yersin, H. *Top. Curr. Chem.* **2004**, *241*, 1. (b) Chou, P.-T.; Chi, Y. *Eur. J. Inorg. Chem.* **2006**, 3319. (c) Chou, P.-T.; Chi, Y. *Chem.—Eur. J.* **2007**, *13*, 380. (d) Williams, J. A. G.; Develay, S.; Rochester, D. L.; Murphy, L. *Coord. Chem. Rev.* **2008**, *252*, 2596.

(2) (a) Baldo, M. A.; O'Brien, D. F.; You, Y.; Shoustikov, A.; Sibley, S.; Thompson, M. E.; Forrest, S. R. *Nature* **1998**, *395*, 151. (b) Lamansky, S.; Djurovich, P.; Murphy, D.; Abdel-Razzaq, F.; Lee, H.-E.; Adachi, C.; Burrows, P. E.; Forrest, S. R.; Thompson, M. E. *J. Am. Chem. Soc.* **2001**, *123*, 4304.

(3) Yang, C.-H.; Cheng, Y.-M.; Chi, Y.; Hsu, C.-J.; Fang, F.-C.; Wong, K.-T.; Chou, P.-T.; Chang, C.-H.; Tsai, M.-H.; Wu, C.-C. *Angew. Chem., Int. Ed.* **2007**, *46*, 2418.

(4) (a) Hwang, F.-M.; Chen, H.-Y.; Chen, P.-S.; Liu, C.-S.; Chi, Y.; Shu, C.-F.; Wu, F.-I.; Chou, P.-T.; Peng, S.-M.; Lee, G.-H. *Inorg. Chem.* **2005**, *44*, 1344. (b) Nazeeruddin, M. K.; Grätzel, M. *Struct. Bonding (Berlin)* **2007**, *123*, 113. (c) Matsushita, T.; Asada, T.; Koseki, S. *J. Phys. Chem. C* **2007**, *111*, 6897. (d) Zhou, G.; Ho, C.-L.; Wong, W.-Y.; Wang, Q.; Ma, D.; Wang, L.; Lin, Z.; Marder, T. B.; Beeby, A. *Adv. Funct. Mater.* **2008**, *18*, 499.

(5) (a) Yang, C.-H.; Li, S.-W.; Chi, Y.; Cheng, Y.-M.; Yeh, Y.-S.; Chou, P.-T.; Lee, G.-H.; Wang, C.-H.; Shu, C.-F. *Inorg. Chem.* **2005**, *44*, 7770. (b) Chang, C.-J.; Yang, C.-H.; Chen, K.; Chi, Y.; Shu, C.-F.; Ho, M.-L.; Yeh, Y.-S.; Chou, P.-T. *Dalton Trans.* **2007**, 1881.

(6) Tamayo, A. B.; Garon, S.; Sajoto, T.; Djurovich, P. I.; Tsyba, I. M.; Bau, R.; Thompson, M. E. *Inorg. Chem.* **2005**, *44*, 8723.


Published on Web 06/19/2009

**Scheme 1.** Inter-Ligand Energy Transfer (ILEnT) Mechanism Taken from Figure 3e in Reference 7c. and Chart 1 in Reference 7d[a]

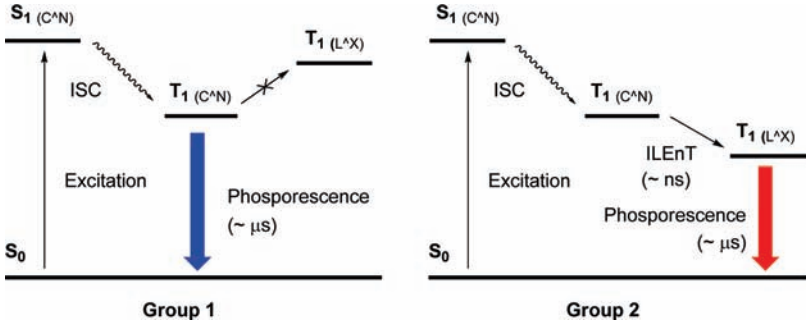


[a] The cyclometalating and anionic chelates are represented by C^N and L^X, respectively; ISC = intersystem crossing.

Parallel to these investigations, an interligand energy transfer (ILEnT)[7] process has recently been proposed by Park and co-workers to illustrate the color tuning from 468 to 666 nm that occurred in the system $[Ir(dfppy)_2(L^X)]$, where dfppy = 2-(2,4-difluorophenyl)pyridinato. Such a wide range tunability is in sharp contrast to the small range of color tuning (< 54 nm) reported by Thompson and co-workers.[8] According to Park and co-workers,[7a] these complexes are categorized into two groups, namely, those anchored by picolininate (group 1) and by quinaldinate, isoquinolinate, and pyrazinate (group 2) L^X chelate. The classification is based on their empirical steady-state observations such as relative emission wavelength, appearance of emission spectral feature in solid state versus that in solution, and different response to solvatochromism, and so on. From the aspect of excited state relaxation, Park and co-workers also reported that group 2 complexes, upon excitation, underwent fast singlet−triplet intersystem crossing, then followed by a much slower, 6−7 ns ILEnT among orbitals that localized on the C^N and L^X chelates (Scheme 1).[7]

As all frontier orbitals of Ir(III) cyclometalated complexes are effectively "cross-talked" via the central metal atom, such a "nanosecond time scale" for internal energy transfer, that is, the internal conversion in conventional description, among the triplet manifolds for group 2 complexes is anomalous and is in sharp contrast to typical time scale of internal conversion of < 10 ps for polyatomic molecules in condensed phase.[9] To clarify as well as to resolve this puzzle, we here conducted comprehensive time-resolved absorption and emission studies using two prototypical complexes; namely, iridium(III) bis[2-(2,4-difluorophenyl)pyridinato-N,$C^{2'}$] quinaldinate (**1**) and iridium(III) bis[2-(2,4-difluorophenyl)pyridinato-$N,C^{2'}$]-[2-(6-methylbenzoxazol-2-yl)phenolate] (**2**) (Scheme 2) that are ascribed to group 2. We combined the picosecond-to-microsecond transient spectroscopy and sub-nanosecond time-resolved fluorescence (decay)/phosphorescence (rise) to gain more insight into the corresponding relaxation dynamics. As a result, our data are in sharp contrast to those reported by Park and co-workers. Details of the results and discussion are elaborated in the following sections.

**Scheme 2.** Structural Drawing of Complexes **1** and **2**

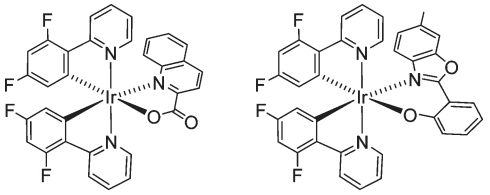


## Experimental Section

**General Procedures.** All reactions were performed under argon atmosphere and solvents were distilled from appropriate drying agents prior to use. Commercially available reagents were used without purification unless otherwise stated. 2-(6-Methylbenzoxazol-2-yl) phenol was prepared according to the literature method.[10] All reactions were monitored using precoated TLC plates (0.20 mm with fluorescent indicator $UV_{254}$). Mass spectra were obtained on a JEOL SX-102A instrument operating in electron impact (EI) or fast atom bombardment (FAB) mode. $^1H$ and $^{13}C$ NMR spectra were recorded on a Varian Mercury-400 or an INOVA-500 instrument. Elemental analysis was carried out with a Heraeus CHN-O Rapid Elementary Analyzer.

**Synthesis of Iridium(III) Bis[2-(2,4-difluorophenyl)pyridinato-N,$C^{2'}$] Quinaldinate (1).** $[(dfppy)_2Ir(\mu\text{-}Cl)]_2$ (0.12 g, 0.10 mmol), $Na_2CO_3$ (0.83 g, 1.00 mmol), and quinoline-2-carboxylic acid (0.04 g, 0.22 mmol) were dissolved in 15 mL of 2-ethoxyethanol. The reaction was refluxed under argon for 8 h. After removal of solvent, the residue was purified by silica gel column chromatography using a 1:1 mixture of ethyl acetate and hexane as the eluent. The pale yellow crystals were obtained by slow diffusion of hexane into a $CH_2Cl_2$ solution at room temperature (RT; 76 mg, 0.10 mmol, 52%).

**Spectral Data of 1.** $^1H$ NMR (400 MHz, $CDCl_3$, 294 K) $\delta$ 5.41 (dd, $J$ = 8.8, 2.0 Hz, 1H), 5.91 (dd, $J$ = 8.4, 2.0 Hz 1H), 6.36−6.51 (m, 2H), 6.83 (t, $J$ = 6.4 Hz, 1H), 7.10 (t, $J$ = 6.4 Hz, 1H), 7.34−7.38 (m, 1H), 7.54−7.58 (m, 2H), 7.67 (t, $J$ = 7.6 Hz, 1H), 7.73 (t, $J$ = 8.0 Hz, 1H), 7.86 (t, $J$ = 9.6 Hz, 2H), 8.16 (d, $J$ = 8.5 Hz, 1H), 8.28 (d, $J$ = 8.4 Hz, 1H), 8.41 (d, $J$ = 8.4 Hz, 1H), 8.51 (d, $J$ = 8.0 Hz, 1H), 8.64 (d, $J$ = 5.6 Hz, 1H). $^{13}C$ NMR

(7) (a) You, Y.; Park, S. Y. *J. Am. Chem. Soc.* **2005**, *127*, 12438. (b) Karatsu, T.; Ito, E.; Yagai, S.; Kitamura, A. *Chem. Phys. Lett.* **2006**, *424*, 353. (c) You, Y.; Kim, K. S.; Ahn, T. K.; Kim, D.; Park, S. Y. *J. Phys. Chem. C* **2007**, *111*, 4052. (d) You, Y.; Seo, J.; Kim, S. H.; Kim, K. S.; Ahn, T. K.; Kim, D.; Park, S. Y. *Inorg. Chem.* **2008**, *47*, 1476. (e) Lu, J.; Liu, Q.; Ding, J.; Tao, Y. *Synth. Met.* **2008**, *158*, 95. (f) You, Y.; Park, S. Y. *Dalton Trans.* **2009**, 1267.

(8) (a) Sajoto, T.; Djurovich, P. I.; Tamayo, A.; Yousufuddin, M.; Bau, R.; Thompson, M. E.; Holmes, R. J.; Forrest, S. R. *Inorg. Chem.* **2005**, *44*, 7992. (b) Li, J.; Djurovich, P. I.; Alleyne, B. D.; Yousufuddin, M.; Ho, N. N.; Thomas, J. C.; Peters, J. C.; Bau, R.; Thompson, M. E. *Inorg. Chem.* **2005**, *44*, 1713.

(9) Birks, J. B. *Photophysics of aromatic molecules*; Wiley-Interscience: London, 1970.

(10) Seo, J.; Kim, S.; Park, S. Y. *J. Am. Chem. Soc.* **2004**, *126*, 11154.

(100 MHz, $CDCl_3$) $\delta$: 97.3, 98.4, 113.7, 114.6, 122.0, 122.5, 122.7, 123.4, 124.7, 127.9, 128.7, 130.6, 131.4, 138.1, 139.6, 146.4, 147.9, 148.7, 149.3, 153.5, 153.7, 159.5, 160.3, 160.5, 162.1, 162.2, 162.9, 164.1, 164.8, 165.1, 171.1, 174.1. MS (FAB): $m/z$ 746 $[M+1]^+$. Anal. Calcd for $C_{32}H_{18}F_4IrN_3O_2$:C, 51.61; H, 2.44; N, 5.64. Found: C, 51.55; H, 2.34; N, 5.80.

**Synthesis of Iridium(III) Bis[2-(2,4-difluorophenyl)pyridinato-N,C$^{2'}$][2-(6-methylbenzoxazol-2-yl) Phenolate] (2).** $[(dfppy)_2Ir(\mu\text{-}Cl)]_2$ (0.121 g, 0.10 mmol), $Na_2CO_3$ (0.830 g, 1.00 mmol), and 2-(6-methylbenzoxazol-2-yl) phenol (0.05 g, 0.22 mmol) were dissolved in 15 mL of 2-ethoxyethanol. The solution was refluxed under argon for 7 h. After removal of solvent, the residue was purified by silica gel column chromatography using a 1:3 mixture of ethyl acetate and hexane as the eluent. The yellow crystals were obtained by slow diffusion of hexane into a $CH_2Cl_2$ solution at RT (98 mg, 0.12 mmol, 62%).

**Spectral Data of 2.** $^1$H NMR (400 MHz, $CDCl_3$, 294 K) $\delta$: 2.35 (s, 3H), 5.57 (dd, $J$ = 8.4, 2.0 Hz, 1H), 5.89 (dd, $J$ = 8.4, 2.0 Hz, 1H), 6.01 (d, $J$ = 8.4 Hz, 1H), 6.35−6.50 (m, 3H), 6.73 (t, $J$ = 8.4 Hz, 2H), 6.87 (t, $J$ = 6.0 Hz, 1H), 7.06 (t, $J$ = 6.0 Hz, 1H), 7.16−7.19 (m, 1H), 7.25 (s, 1H), 7.67 (t, $J$ = 8.0 Hz, 2H), 7.92 (dd, $J$ = 8.0, 1.6 Hz, 1H), 8.06 (d, $J$ = 6.4 Hz, 1H), 8.17 (d, $J$ = 8.4 Hz, 1H), 8.25 (d, $J$ = 8.4 Hz, 1H), 8.81 (d, $J$ = 5.6 Hz, 1H). $^{13}$C NMR (100 MHz, $CDCl_3$) $\delta$: 21.4, 97.0, 97.9, 110.3, 110.5, 113.7, 114.1, 115.6, 117.5, 121.9, 122.4, 123.1, 125.3, 126.0, 128.6, 133.6, 135.4, 137.7, 138.5, 148.9, 149.1, 149.5, 153.1, 155.0, 159.6, 159.7, 160.2, 161.6, 161.8, 162.1, 162.7, 164.1, 164.3, 165.0, 165.4, 168.9. MS (FAB): $m/z$ 798 $[M+1]^+$. Anal. Calcd for $C_{36}H_{22}F_4IrN_3O_2$: C, 54.27; H, 2.78; N, 5.27. Found: C, 54.36; H, 2.67; N, 5.35.

**Spectroscopic and Lifetime Measurements.** Steady-state absorption and emission spectra were recorded on a Hitachi (U-3310) spectrophotometer and an Edinburgh (FS920) fluorimeter, respectively. Both wavelength-dependent excitation and emission response of the fluorimeter have been calibrated. The various solvents were of spectragrade quality (Merck Inc.) and were used right after being received.

Coumarin 480 in ethanol with an emission yield of $\Phi \sim 0.95$[11] ($\lambda_{max}$ = 471 nm, Exciton) was used as reference to determine quantum yields for the studied compounds in solution. Equation 1 was used to calculate the emission quantum yields.

$$\Phi_s = \Phi_r \left( \frac{\eta_s^2 A_r I_s}{\eta_r^2 A_s I_r} \right) \quad (1)$$

In Equation 1, $\Phi_s$ and $\Phi_r$, are the quantum yields of the unknown and reference samples, $\eta$ is the refractive index of the solvent, $A_r$ and $A_s$ are the absorbance of the reference and the unknown samples at the excitation wavelength, and $I_s$ and $I_r$ are the integrated areas under the emission spectra of interest, respectively.

Emission lifetime studies were performed by an Edinburgh FL900 photon-counting system with a femtosecond Ti-Sapphire laser as the light source. In this setup, a Ti-Sapphire oscillator (80 MHz, Spectra-Physics) coupled with a regenerative amplifier (Spitfire Pro, Spectra-Physics) that produces 120 fs laser pulses at 800 nm with a 1 kHz repetition rate was employed, and then used to produce second harmonic (400 nm) as an excitation source. During the acquisition, we kept the counting rate of the photon counting detector around 10−50 Hz. The counts obtained in the peak channel are 200 counts, and the corresponding data acquisition time is 3−5 h. The dark noise of PMT has been minimized by cooling down PMT to −20 °C during measurements, together with the optimization of TAC (Time to Amplitude Convertor) threshold.

Data were analyzed using a nonlinear least-squares procedure in combination with an iterative convolution method. The emission decays were analyzed by the sum of exponential functions, which allows partial removal of the instrument time broadening and consequently renders a temporal resolution of 300 ps.

**Transient Absorption Measurements.** The femto-picosecond transient absorption measurements were performed according to previous reports.[12,13] However, the system has been modified to improve the sensitivity and stability. In detail, a Spitfire Pro system (Spectra-Physics) was used as the laser source. This system comprises a seed laser, a pump laser, a stretcher, a Ti:sapphire regenerative amplifier, and a compressor. The output of the system consists of pulses of 800 nm, 1 W, 120 fs (fwhm) at a repetition rate of 1 kHz. The pump−probe spectroscopic setup is then based on an ExciPro spectrometer (CDP System Corp). The Spitfire Pro output is first split (50%) into two beams, in which the pump is converted to designated excitation wavelengths by coupling it into a second-harmonic generator (for 400 nm excitation). The probe is first passed through a computer-controlled delay line, and then focused on a 1 mm thick sapphire plate to generate a white light continuum (350−1000 nm). The pump beam is then passed through a computer controlled optical chopper, and focused (3 mm) on the sample cell. The sample cell is a 1 mm optical path quartz cylindrical cell placed in a variable-speed rotating holder. The white light probe beam is collimated and focused into the sample cell, superimposed to the pump beam at an angle of about 5°. To minimize the temporal chirp in the spectrum, parabolic mirrors are used for focus and collimation. After passing through the sample cell, the white continuum is coupled into a 100 $\mu$m optical fiber connected to a diode array. Typically, time-resolved absorption spectra were acquired averaging over 200 excitation pulses at any delay time. With 120 fs pump and probe pulses, the effective time resolution of the ultrafast spectrometer, that is, the risetime of an "instantaneous" signal, is about 220 fs. The maximum temporal window of the experiment, limited by the optical delay stage, is 0−500 ps.

Nano-microsecond transient absorption spectrum was recorded with a laser flash photolysis system (Edinburgh LP920),[14−16] in which the third harmonic (355 nm) of an Nd:YAG laser at 10 Hz and a white light square pulse were used as pump and probe beams, respectively. These two pulses were crossed at a 90° angle with an overlapping distance of 10 mm. The temporal resolution was limited by the excitation pulse duration of 8 ns.

**Computational Methodology.** All calculations were carried out by using a Gaussian 03 (G03) program package.[17] Calculations on the electronic ground state of complexes **1** and **2** were

(11) Jones, G.; Jackson, W. R.; Choi, C. Y.; Bergmark, W. R. *J. Phys. Chem.* **1985**, *89*, 294.

(12) Chou, P. T.; Chen, Y. C.; Yu, W. S.; Cheng, Y. M. *Chem. Phys. Lett.* **2001**, *340*, 89.

(13) Chou, P. T.; Chen, Y. C.; Yu, W. S.; Chou, Y. H.; Wei, C. Y.; Cheng, Y. M. *J. Phys. Chem. A* **2001**, *105*, 1731.

(14) Chou, P. T.; Wu, G. R.; Liu, Y. I.; Yu, W. S.; Chiou, C. S. *J. Phys. Chem. A* **2002**, *106*, 5967.

(15) Chen, C. T.; Lin, J. S.; Kuo, J. H.; Weng, S. S.; Cuo, T. S.; Lin, Y. W.; Cheng, C. C.; Huang, Y. C.; Yu, J. K.; Chou, P. T. *Org. Lett.* **2004**, *6*, 4471.

(16) Thanasekaran, P.; Liao, R. T.; Manimaran, B.; Liu, Y. H.; Chou, P. T.; Rajagopal, S.; Lu, K. L. *J. Phys. Chem. A* **2006**, *110*, 10683.

(17) Frisch, M. J.; Trucks, G. W.; Schlegel, H. B.; Scuseria, G. E.; Robb, M. A.; Cheeseman, J. R.; Montgomery, J. A.; Vreven, Jr. T.; Kudin, K. N.; Burant, J. C.; Millam, J. M.; Iyengar, S. S.; Tomasi, J.; Barone, V.; Mennucci, B.; Cossi, M.; Scalmani, G.; Rega, N.; Petersson, G. A.; Nakatsuji, H.; Hada, M.; Ehara, M.; Toyota, K.; Fukuda, R.; Hasegawa, J.; Ishida, M.; Nakajima, T.; Honda, Y.; Kitao, O.; Nakai, H.; Klene, M.; Li, X.; Knox, J. E.; Hratchian, H. P.; Cross, J. B.; Bakken, V.; Adamo, C.; Jaramillo, J.; Gomperts, R.; Stratmann, R. E.; Yazyev, O.; Austin, A. J.; Cammi, R.; Pomelli, C.; Ochterski, J. W.; Ayala, P. Y.; Morokuma, K.; Voth, G. A.; Salvador, P.; Dannenberg, J. J.; Zakrzewski, V. G.; Dapprich, S.; Daniels, A. D.; Strain, M. C.; Farkas, O.; Malick, D. K.; Rabuck, A. D.; Raghavachari, K.; Foresman, J. B.; Ortiz, J. V.; Cui, Q.; Baboul, A. G.; Clifford, S.; Cioslowski, J.; Stefanov, B. B.; Liu, G.; Liashenko, A.; Piskorz, P.; Komaromi, I.; Martin, R. L.; Fox, D. J.; Keith, T.; Al-Laham, M. A.; Peng, C. Y.; Nanayakkara, A.; Challacombe, M.; Gill, P. M. W.; Johnson, B.; Chen, W.; Wong, M. W.; Gonzalez, C.; Pople, J. A.; *Gaussian 03*, Revision C.02; Gaussian, Inc.: Wallingford, CT, 2004.

carried out by using the DFT method with B3LYP density functional theory.[18,19] The Hay−Wadt double-ζ with a Los Alamos relativistic effect core potential basis set LANL2DZ[20] was employed for the iridium atom, and other atoms were described by a split valence Pople basis (6-31G*).[21] The relativistic effective core potential (ECP) replaced the inner core electrons of Ir(III) atom, leaving the outer core ($5s^25p^6$) electrons and the $5d^6$ valence electrons. The basis set was described as Ir (8s6p3d)/[3s3p2d], C, N, O, and F (10s,4p,1d)/[3s,2p,1d], and H (4s)/[2s]. On the basis of the optimized geometry in the ground state, the absorption and emission properties in $CH_2Cl_2$ can be calculated by TD-DFT[22] with the polarized continuum model (PCM), as implemented in G03. Within TD-DFT, the description of the excited states is based on a linear combination of singly occupied-to-virtual orbital excitations and thereby provides information beyond a simple HOMO−LUMO picture. Compositions of molecular orbitals, overlap populations between molecular fragments, bond orders, and density-of-states spectra were calculated by using the AOMix program.[23] For the characterization of the HOMO-$x$ → LUMO+$y$ transitions as partial charge transfer (CT) transitions, the following definition of the CT character[24] has been used:

$$\mathrm{CT(M)} = \%\mathrm{(M)HOMO}-x - \%\mathrm{(M)LUMO}+y \qquad (2)$$

Here %(M)HOMO−$x$ and %(M)LUMO+$y$ are electronic densities on the metal in HOMO−$x$ and LUMO+$y$. If the excited state, for example, $S_1$ or $T_1$, is formed by more than one one-electron excitation, then the metal CT character of this excited-state is expressed as a sum of CT characters of each participating excitation, $i \rightarrow j$:

$$\mathrm{CT}_I\mathrm{(M)} = \sum_{i,a} [C_I(i \rightarrow j)]^2 (\%(\mathrm{M})_i - \%(\mathrm{M})_j) \qquad (3)$$

Here $C_I(i \rightarrow j)$ are the appropriate coefficients of the $I$th eigenvector of the CT matrix. Accordingly, one can very effectively use the MO compositions in terms of fragment orbital contributions to probe the nature of electronic transitions.

## Results and Discussion

Prior to the spectroscopic and dynamic measurements, we fully realized that any trace of fluorescence impurity, because of its much higher transition moment than that of the phosphorescence, may dominate the early part of relaxation dynamics, leading to misinterpretation. We have then purified compounds **1** and **2** by repeated recrystallization. Figure 1 reveals UV/vis absorption and emission spectra recorded in $CH_2Cl_2$, while the pertinent data are listed in Table 1. Note that the difference in the photophysical properties, such as emission feature as well as energy gap, between **1** and **2** is mainly due to different L^X ligands

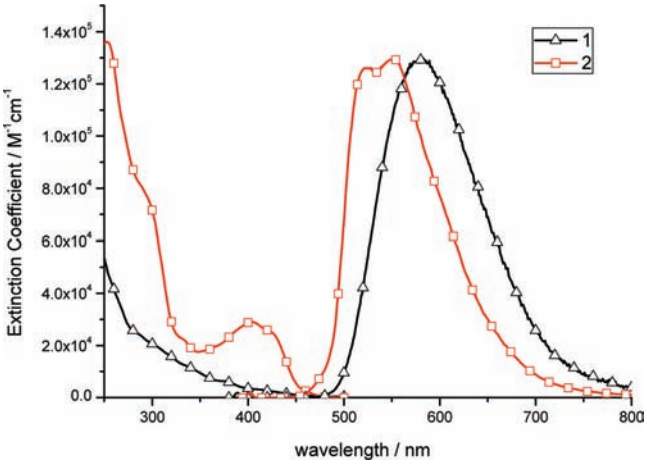


**Figure 1.** UV/vis absorption and normalized emission spectra of **1** and **2** in degassed $CH_2Cl_2$ at room temperature.

(vide infra). As depicted in Figure 1, complexes **1** and **2** in a degassed solution of $CH_2Cl_2$ at 298 K display phosphorescent peak wavelengths at 581 and 526 nm, respectively, the spectral features of which are similar to those reported in previous studies.[7c,7d] The excitation spectra are promptly checked and identical to their corresponding absorption spectra. Their genuine identity therefore confirms the emission originating from **1** and **2** intrinsically, excluding any involvement of impurity. In degassed $CH_2Cl_2$, the observed lifetime of 1.73 and 10.24 μs, together with their measured quantum yield of 0.27 and 0.6, deduces a radiative decay rate constant ($k_r$) of $1.56 \times 10^5\ s^{-1}$ and $5.86 \times 10^4\ s^{-1}$ for **1** and **2**, respectively. The results, in combination with a significant $O_2$ quenching effect, warrant the unambiguous assignment of phosphorescence.

As shown in Figure 2, the dynamics of **1** was monitored at 510 and 600 nm, revealing single-exponential kinetics with a lifetime of 1.73 μs and a system response rise component of < 300 ps. Note that our time-correlated photon counting system consists of a femtosecond (120 fs) Ti-Sapphire laser with a 1 kHz repetition rate. However, limited by the detector response, a temporal resolution of ~300 ps was achieved (see Experimental Section for details). Realizing that the fluorescence, if there is any, should fall in the region of < 500 nm, we then monitored the emission at 460−480 nm ($\lambda_{ex}$ = 400 nm) and only obtained an instrument response limited rise and decay profile (see Figure 2c). Similar results were also obtained for **2** in $CH_2Cl_2$ upon 400 nm excitation, for which the decay of **2** monitored at 500 nm and at 630 nm both are single exponential with system response limited risetime (< 300 ps), as shown in Figure 3.

Thus, the emission of both **1** and **2** measured with a system of 300 ps resolution indicate that neither decay of the fluorescence nor rise of the phosphorescence exhibits nanosecond kinetics. Instead, following Franck−Condon excitation, the time scale required to populate the lowest triplet state, as measured by the rise of phosphorescence, should be ≪ 300 ps. Thus, we failed to provide evidence in supporting the proposed "nanosecond ILEnT process".[7c,7d]

To gain further insight into the excited-state dynamics, femtosecond transient absorption spectroscopy was then carried out. Figure 4 depicts the transient absorption spectra of **1** recorded at selected time delays after excitation at 400 nm in $CH_2Cl_2$. The spectra, in all, reveal a broadband

(18) Lee, C.; Yang, W.; Parr, R. G. *Phys. Rev. B* **1988**, *37*, 785.
(19) Becke, A. D. *J. Chem. Phys.* **1993**, *98*, 5648.
(20) (a) Hay, P. J.; Wadt, W. R. *J. Chem. Phys.* **1985**, *82*, 270. (b) Wadt, W. R.; Hay, P. J. *J. Chem. Phys.* **1985**, *82*, 284. (c) Hay, P. J.; Wadt, W. R. *J. Chem. Phys.* **1985**, *82*, 299.
(21) Hariharan, P. C.; Pople, J. A. *Mol. Phys.* **1974**, *27*, 209.
(22) (a) Jamorski, C.; Casida, M. E.; Salahub, D. R. *J. Chem. Phys.* **1996**, *104*, 5134. (b) Petersilka, M.; Grossmann, U. J.; Gross, E. K. U. *Phys. Rev. Lett.* **1996**, *76*, 1212. (c) Bauernschmitt, R.; Ahlrichs, R.; Hennrich, F. H.; Kappes, M. M. *J. Am. Chem. Soc.* **1998**, *120*, 5052. (d) Casida, M. E. *J. Chem. Phys.* **1998**, *108*, 4439. (e) Stratmann, R. E.; Scuseria, G. E.; Frisch, M. J. *J. Chem. Phys.* **1998**, *109*, 8218.
(23) (a) Gorelsky, S. I. *AOMix, Program for Molecular Orbital Analysis*; University of Ottawa: Ottawa, Canada, 2007; http://www.sg-chem.net. (b) Gorelsky, S. I.; Lever, A. B. P. *J. Organomet. Chem.* **2001**, *635*, 187.
(24) Vlček, A. Jr.; Záliš, S. *Coord. Chem. Rev.* **2007**, *251*, 258.

**Table 1.** Photophysical Properties[a] for **1** and **2**

| | UV/vis [nm]($\varepsilon\times10^{-3}$) | PL $\lambda_{max}$ [nm] | $\Phi$ [%] | $\tau_{obs}$ [$\mu$s] | $k_r$ ($s^{-1}$) | $k_{nr}$ ($s^{-1}$) |
|---|---|---|---|---|---|---|
| **1** | 285 (24.6), 334 (12.4), 375 (6.3) | 581 | 0.27 | 1.73 | $1.56\times10^5$ | $4.22\times10^5$ |
| **2** | 293 (78.0), 404 (29.1), 428 (23.9) | 526, 549 | 0.60 | 10.24 | $5.86\times10^4$ | $3.91\times10^4$ |

[a] Data were recorded in a degassed $CH_2Cl_2$ solution (via three freeze−pump−thaw cycles) at room temperature with $\varepsilon$ in $M^{-1}\cdot cm^{-1}$.

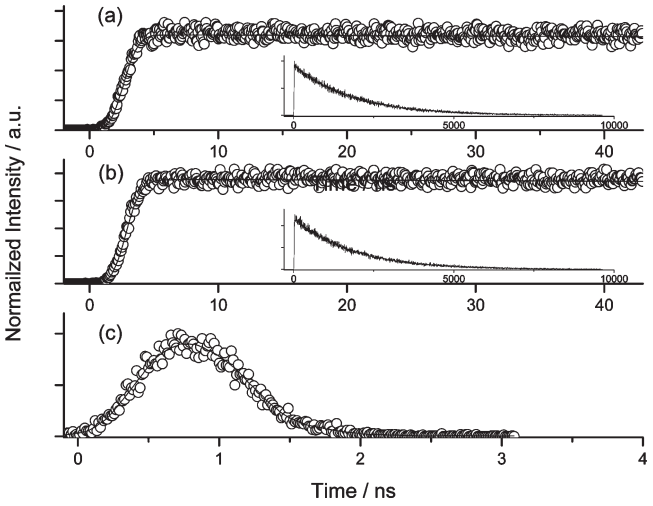


**Figure 2.** Emission decay curves of **1** in degassed $CH_2Cl_2$ excited at 400 nm (~120 fs), monitored at (a) 510 nm, (b) 600 nm, and (c) 470 nm. The solid line is the fit of the experimental data (circles) with an exponential function. Note that the result in (c) is the instrument response with temporal resolution of ~300 ps after deconvolution.

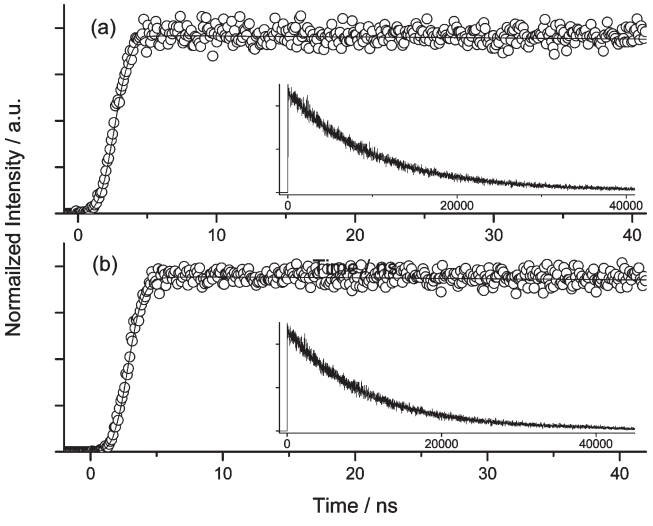


**Figure 3.** Emission decay curves of **2** in degassed $CH_2Cl_2$ excited at 400 nm (~120 fs), monitored at (a) 500 nm, and (b) 630 nm. The solid line is the fit of the experimental data (circles) with an exponential function.

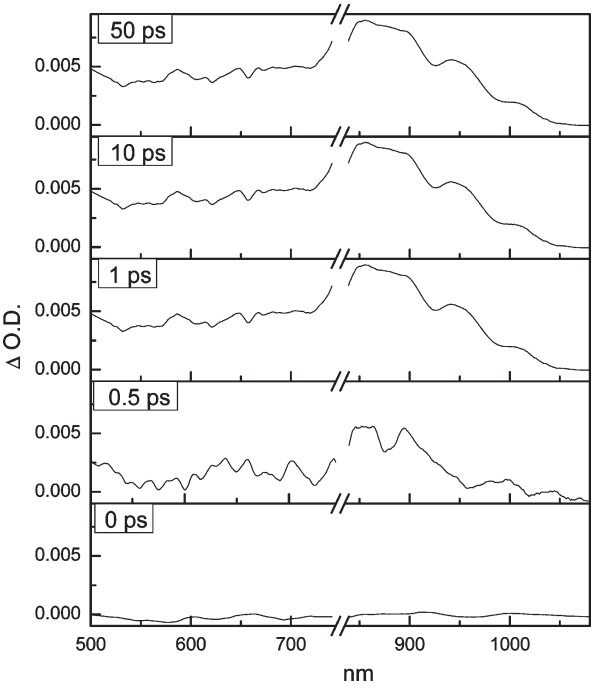


**Figure 4.** Femtosecond transient absorption spectra of **1** in $CH_2Cl_2$ measured following excitation at 400 nm. The disconnected region is due to the second order of laser scattering light.

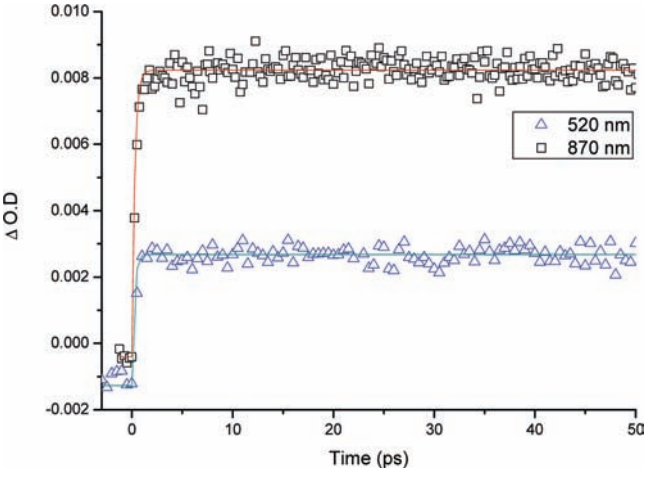


**Figure 5.** Transient absorption kinetics measurement of **1** in $CH_2Cl_2$ following ~120 fs excitation at 400 nm. The probe wavelengths are indicated on the figure. The solid line is the fit to the experimental data (triangles and squares) with an exponential function.

absorption ranging from 500 to 1080 nm, together with an intense absorption at ~870 nm. Obviously, except for minor variation of peak intensities at < 550 nm, which is possibly due to the vibronic/solvent relaxation, the spectral features at > 500 nm remains unchanged after a pump−probe delay time of few picoseconds. The plot of transient absorbance at 520 and 870 nm versus the probe delay time is then shown in Figure 5. The result clearly reveals that the transient absorbance had established immediately within the time scale of < 1 ps after Franck−Condon excitation. The signal then remains unchanged during the entire measurement time window of 500 ps. In fact, for complex **1**, the overlay between the transient spectrum acquired at, for example, 500 ps (femto-system) and the 10 ns (nano-system) data collected on **1** at the spectral range of < 700 nm (the detection limit of current nano-system) is essentially superimposed within the

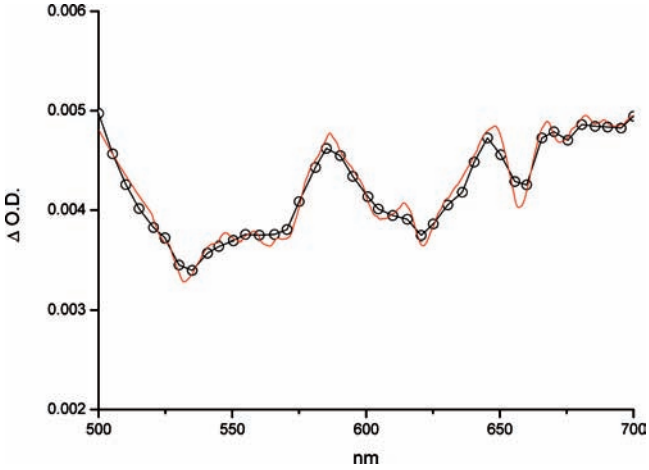


**Figure 6.** Overlay of the transient absorption spectrum of **1** obtained at a pump−probe delay time of 500 ps (solid red line, $\lambda_{ex}$ = 400 nm) and the transient absorption spectrum acquired after 10 ns photoexcitation (circle black line, $\lambda_{ex}$ = 355 nm).

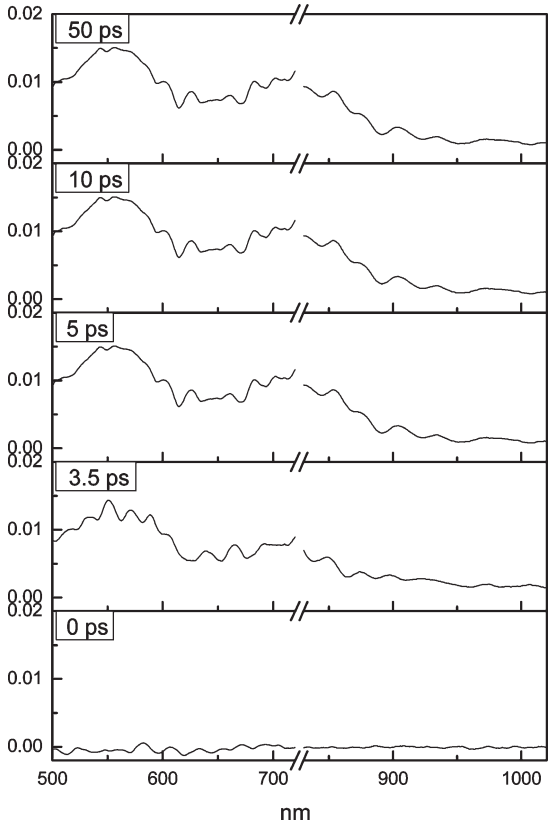


**Figure 7.** Femtosecond transient absorption spectra of **2** in $CH_2Cl_2$ measured following ~120 fs excitation at 400 nm. The disconnected region is due to the second order of laser scattering light.

noise level (see Figure 6). Thus, it seems unambiguous to assign the transient absorption at > few picoseconds to the $T_1$-$T_n$ transition.

Likewise, as shown in Figure 7, in the early time scale of 0−5 ps, the transient absorption of complex **2** appears to have certain changes on the spectral feature, which are possibly due to the solvent induced vibrational relaxation. After 5 ps delay time, however, the transient spectral feature, having a peak wavelength at ~560 nm, remains unchanged throughout the measurement time scale of ~500 ps. Upon

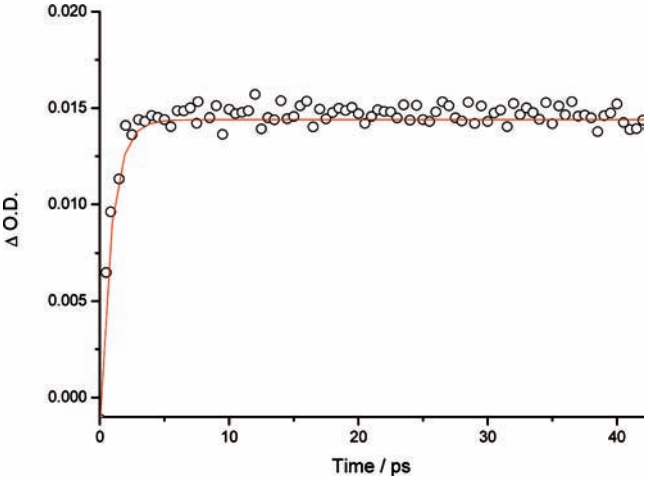


**Figure 8.** Transient absorption kinetics measurement of **2** in $CH_2Cl_2$ following excitation at 400 nm. The probe wavelength is 560 nm. The solid line is the fit to the experimental data (circles) with an exponential function.

monitoring at the peak of 560 nm, the plot of transient absorbance versus the probe delay time displays a fast rise of < 1 ps (see Figure 8).

For both complexes **1** and **2**, because the excitation wavelength of 400 nm being selected is near the onset of the $S_0$-$S_1$ transition, the internal conversion as well as vibrational relaxation in singlet manifold has been minimized. Accordingly, the time scale of < 1 ps for the rise of the triple state implies $S_1 \rightarrow T_n$ intersystem crossing to be ultrafast. This ultrafast time scale is consistent with those transition-metal complexes, for which the lower lying transitions involve certain degrees of MLCT contribution.[25−28] The involvement of metal $d_\pi$ orbitals in these complexes leads to a large first-order spin−orbit coupling constant, resulting in a drastic enhancement of intersystem crossing.

The time-resolved experiment has been repeated several times, and the presented data are consistent and reproducible. One might argue that higher energy excitation such as 355 nm used in previous studies[7c,7d] may result in different relaxation dynamics in the triplet manifold. To check this, we also use 355 nm ($H_2$ pulse lamp) excitation coupled with a time-resolved acquisition system, and the overall system response is ~300 ps. Again, a system limited rise (< 300 ps, not shown here) of phosphorescence was acquired. Besides, independent of the Franck−Condon excitation wavelength, after, for example, few picoseconds, intersystem crossing should take place from the $S_1$ state because of the fast (< few picoseconds) $S_n \rightarrow S_1$ internal conversion coupled with vibrational relaxation.

Therefore, we unfortunately could not reproduce the nanosecond ILEnT process in the triplet manifold reported in literature.[7c,7d] Instead, as shown in Scheme 3, after $S_0 \rightarrow S_1$ (e.g., 400 nm) Franck−Condon excitation,

(25) (a) Damrauer, N. H.; Cerullo, G.; Yeh, A.; Boussie, T. R.; Shank, C. V.; McCusker, J. K. *Science* **1997**, *275*, 54. (b) Damrauer, N. H.; McCusker, J. K. *J. Phys. Chem. A* **1999**, *103*, 8440.
(26) Tang, K.-C.; Liu, K. -L.; Chen, I.-C. *Chem. Phys. Lett.* **2004**, *386*, 437.
(27) Hedley, G. J.; Ruseckas, A.; Samuel, I. D. W. *Chem. Phys. Lett.* **2008**, *450*, 292.
(28) Hedley, G. J.; Ruseckas, A.; Samuel, I. D. W. *J. Phys. Chem. A* **2009**, *113*, 2.

**Scheme 3.** Proposed Potential Energy Diagram of Ir(III) Metal Complexes **1** and **2**[a]

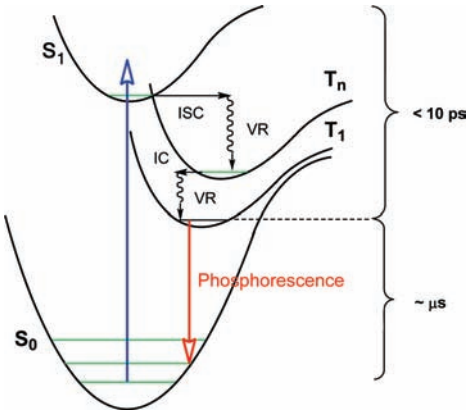


[a] IC = internal conversion; ISC = intersystem crossing; VR = vibrational relaxation.

the results of femto- to nanosecond dynamics render a rapid $S_1$-$T_n$ rate of intersystem crossing ( < 1 ps for **1** and **2**), followed by the < 10 ps of $T_n \rightarrow T_1$ internal conversion and/or $T_1$ ($v = m \rightarrow v = 0$) vibrational relaxation. Such a relaxation mechanism follows the fundamental basis of photophysics. Because of the MLCT contribution in the lower lying transitions, significant spin−orbit coupling takes place. As a result, $S_1$ should largely mix with triplet character and vice versa for $T_n$ (or $T_1$), such that the forbidden $S_1 \rightarrow T_n$ intersystem crossing becomes allowed, and there is no surprise regarding the ultrafast rate of intersystem crossing. Once populated at the triplet manifold, the $T_n \rightarrow T_1$ internal conversion and subsequent vibrational relaxation to populate at the $T_1$ zero vibrational level must be fast ($\ll$ ns, and is < 10 ps in cases of **1** and **2**) because of its spin allowed process with smaller energy gap in the excited state. This latter process is independent of the L^X chromophores, that is, having no relationship with inter- or intraligand energy transfer, because all frontier orbitals involved for **1** and **2**, to certain extents, are coupled via the metal $d_\pi$ orbitals.

The use of the femtosecond laser as excitation source shows promise for better resolution than that reported by Park and co-workers[7c,7d] in both time-resolved spectra and relaxation dynamics. Regarding the controversy in dynamics between ours and previous results, first, our longstanding experience has led us to believe that it is always subject to much uncertainty when the relaxation dynamics, which is buried inside the system response function, are to be extracted.[14−16] Under the circumstance that nanosecond Q-switched Nd:YAG laser (Continuum, Surelite) was employed as excitation,[7c,7d] previous relaxation dynamics resolved require more rigorous examination under shorter time scale. Second, we also realized that the crude products of both complexes **1** and **2** contain trace amount of unidentified impurity. Although the emission associated with such impurity was not observable in steady state measurement, because of the much higher transition moment, its respective fluorescence may be commonly observed. To exclude such possible contamination, both complexes **1** and **2** were repeatedly recrystallized before time-resolved experiments. As a consequence, the data in our emission lifetime and transient absorption measurements are complementarily supported, leading to a revised relaxation dynamics depicted in Scheme 3 without ambiguity. Note that it is yet unclear what the source of the discrepancy between the present time-resolved spectroscopy results and the previously reported results of Park and co-workers is, and further work is needed to fully resolve this issue.

Another angle between groups 1 and 2 luminescent Ir complexes can be viewed via computational approaches. As depicted in Supporting Information, Figure S1, $T_1$ of **1** and **2** (group 2) and **FIrpic** (group 1)[7a] all involve a significant $\pi\pi^*$ transition, consisting of intraligand charge transfer and ligand-to-ligand charge transfer. Their $S_0 \rightarrow T_1$transitions are contributed by the C^N cyclometalated ligands and the introduced quinaldinate (**1**), 2-(6-methylbenzoxazol-2-yl)-phenolate (**2**) or picolinate (**FIrpic**) ligand, together with slightly different extents metal-to-ligand charge transfer (MLCT) transition (see Supporting Information, Table S1). Thus, similar transition character was expected in $T_1$ for both classes of complexes. Likewise, the transition characters of the singlet state for **1**, **2**, and **FIrpic** do not reveal notable difference from the corresponding lowest triplet states (see Supporting Information, Table S1). Thus, there seems to be no fundamental differences between groups 1 and 2 complexes. As for the spectroscopic interpretation, for group 2 complexes,[7] the exceeding large $\pi\pi^*$ energy gap of the dfppy ligands makes LUMO located in part at the L^X ligand. The addition of electron withdrawing (or releasing) groups at this site would display a significant decrease (or increase) of the LUMO energy level. In other words, this class of complexes allows the L^X ligand dominating the lowest lying excited state.[5b] On the other hand, group 1 complexes such as **FIrpic**[7a,29] and relevant derivatives[30] display blue-shifted emissions simply because their LUMOs, to certain extents, are located on the cyclometalated dfppy ligands (see Supporting Information, Figure S1), possessing a higher energy level. Thus, the tuning of emissions in these heteroleptic Ir(III) complexes can be illustrated without invoking the ILEnT mechanism.

## Conclusion

In this study, the excited state evolutions of two heteroleptic Ir(III) complexes **1** and **2** were investigated using time-correlated single photon counting and femto-picosecond transient absorption spectroscopy. Several remarks can be summarized according to our results: (1) The phosphorescence for both **1** and **2** consists of a system response limited rise (<300 ps) and a single exponential decay. (2) Femto-picosecond transient absorption acquired in room temperature $CH_2Cl_2$ reveals an ultrafast $S_1 \rightarrow T_n$ intersystem crossing (<1 ps) and a rapid $T_n \rightarrow T_1$ internal conversion/vibrational relaxation within a time period of < 10 ps. We thus conclude the absence of nanosecond ILEnT process[7] for **1** and **2**. Instead, following Franck−Condon excitation, the time scale required to populate the lowest triplet state should be <10 ps.

(29) Gu, X.; Fei, T.; Zhang, H.; Xu, H.; Yang, B.; Ma, Y.; Liu, X. *J. Phys. Chem. A* **2008**, *112*, 8387.

(30) (a) Chang, C.-F.; Cheng, Y.-M.; Chi, Y.; Chiu, Y.-C.; Lin, C.-C.; Lee, G.-H.; Chou, P.-T.; Chen, C.-C.; Chang, C.-H.; Wu, C.-C. *Angew. Chem., Int. Ed.* **2008**, *47*, 4542. (b) Chiu, Y.-C.; Chi, Y.; Hung, J.-Y.; Cheng, Y.-M.; Yu, Y.-C.; Chung, M.-W.; Lee, G.-H.; Chou, P.-T.; Chen, C.-C.; Wu, C.-C.; Hsieh, H.-Y. *ACS Appl. Mater. Int.* **2009**, *1*, 433. (c) Chiu, Y.-C.; Hung, J.-Y.; Chi, Y.; Chen, C.-C.; Chang, C.-H.; Wu, C.-C.; Cheng, Y.-M.; Yu, Y.-C.; Lee, G.-H.; Chou, P.-T. *Adv. Mater.* **2009**, *21*, 2221.

Our results as a whole can be explained without overturning long-established photophysical principles. We believe that understanding these dynamic relaxations would elaborate the transition processes in OLED emitters, and hence facilitate their future development.

**Acknowledgment.** We thank the National Science Council for financial support and the National Center for High-Performance Computing for computer time and facilities.

**Supporting Information Available:** Calculated energy levels, orbital transition analyses, and the figures of frontier orbitals at $S_0$ optimized geometry of **1**, **2** and **FIrpic**. This material is available free of charge via the Internet at http://pubs.acs.org.